JOURNAL OF GEOPHYSICAL RESEARCH, VOL. 94, NO. B5, PAGES 5716–5728, MAY 10, 1989

Tomographic Inversion for Three-Dimensional Velocity Structure at Mount St. Helens Using Earthquake Data

JONATHAN M. LEES AND ROBERT S. CROSSON

Geophysics Program, University of Washington

Tomographic inversion is applied to 17,659 *P* phase observations at 21 stations from 2023 earthquakes in the vicinity of Mount St. Helens to study the three-dimensional velocity structure. Block size for the inversion is 2 km horizontally and 2 km or more vertically. Locations of hypocenters are assumed known and are based on a reference one-dimensional, layered velocity structure. A conjugate gradient technique (LSQR) is used to invert the large sparse system of equations, augmented by regularization with a Laplacian roughening matrix. Resolution is estimated by computing the impulse response of the inversion for various critical locations, and uncertainties of the estimates are determined by a jackknife approach. The results of the inversion show a remarkable correlation with known geological and geophysical features. The Spirit Lake and Spud Mt. plutons are characterized by high-velocity regions extending to approximately 9 km depth. The St. Helens seismic zone, a band of diffuse seismicity extending NNW from the volcano is evident as a prominent low-velocity lineation. The change in character of the velocity anomalies south of St. Helens corresponds well with the near cessation of seismic activity there. A low-velocity anomaly beneath the crater from 6 to 16 km depths may represent modern magma accumulations.

INTRODUCTION

Since the explosive eruptions of May 1980, the Mount St. Helens region (Figure 1) has generated intense interest and speculation regarding the nature of volcanic activity in relationship to subduction in the Pacific Northwest. It is imperative to know the location of magmatic sources, the conduits and transport systems that supply the volcanos, and their relation to adjacent geologic structure if we attempt to determine constraints on the placement of volcanic activity in the Cascade range. While surface geological studies [e.g., *Evarts et al.*, 1987; *Mullineaux and Crandell*, 1981; *Phillips*, 1987; *Swanson and Clayton*, 1983; *Hammond*, 1980] are useful in determining some of the features present, extensive erosion, lava coverage, and forestation impede a clear understanding of the complex structures in this region. Subtle variations in rock properties are measurable by various geophysical means, and they remain important avenues for exploring this problem.

The geology of the Mount St. Helens region is summarized in reports by *Evarts et al.* [1987], *Finn and Williams* [1987], *Williams et al.* [1987], and *Stanley et al.* [1987]. The region is dominated by a succession of tectonic, igneous, and erosional events that determined the present complex of basalts, andesites, and quartz-diorite that are exposed at the surface. Forearc basins were present beginning in the late Jurassic to early Cretaceous, and frontal arcs have been compressed against the continental margin since the early Miocene [*Dickinson*, 1976]. During the Eocene, volcanism was intermittent, but in the Oligocene and early Miocene there was a continuous span of volcanic activity [*Evarts et al.*, 1987] resulting by mid-Miocene in a well-defined line of composite volcanos. The modern range of Cascade volcanos dates to approximately 1 Ma and Mount St. Helens itself began producing dacitic lavas about 40,000 years ago [*Mullineaux and Crandell*, 1981]. In the mid-Miocene there were periods of extensive plutonism when the Spirit Lake and Spud Mountain plutons of quartz-diorite were intruded north of Mount St. Helens [*McBirney*, 1978]. To the southwest of St. Helens there appears to be a series of dacite plug domes that predate the modern volcano [*Mullineaux and Crandell*, 1981]. Ten kilometers to the SSE lies the extinct Marble Mountain volcano, one of several late Pleistocene volcanos that have erupted in close vicinity to Mount St. Helens [*Williams et al.*, 1987].

Several geophysical studies have recently been published focusing on the Mount St. Helens region [*Finn and Williams*, 1987; *Williams et al.*, 1987; *Stanley et al.*, 1987; *Weaver and Smith*, 1983], in attempts to clarify the tectonics and to delineate subsurface geologic features. Analysis of aeromagnetic data [*Finn and Williams*, 1987] and gravity data [*Williams et al.*, 1987] indicates the presence of an anomalous, intrusive unit beneath the present volcano. Using conductivity data, *Stanley et al.* [1987] concluded that this anomalous unit overlies a unit of sedimentary rocks described by *Dickinson* [1976]. *Stanley et al.* [1987] further describe a large conductivity anomaly that trends north of St. Helens paralleling the so called St. Helens seismic zone (SHZ) as defined by *Weaver and Smith* [1983].

In this paper, we use the vast amount of seismic data collected in the Mount St. Helens region to perform a three-dimensional tomographic inversion of *P* wave velocity variations. The resulting three-dimensional model shares several characteristics of the other geophysical and geological analyses mentioned above and determines, within the resolution limits of the data, the lateral and vertical extent of some of the anomalies cited

METHOD OF INVERSION

We follow the usual method for linearization and discretization that is commonly used in seismic tomography [*Humphreys et al.*, 1984; *Hearn and Clayton*, 1986; *Nakanishi*, 1985; *Aki et al.*, 1977]. The target region is divided into small blocks within which the slowness perturbations are assumed to be constant. The locations of the earthquakes are determined independently,

Paper number 89JB00008.
0148-0227/89/89JB-00008$05.00

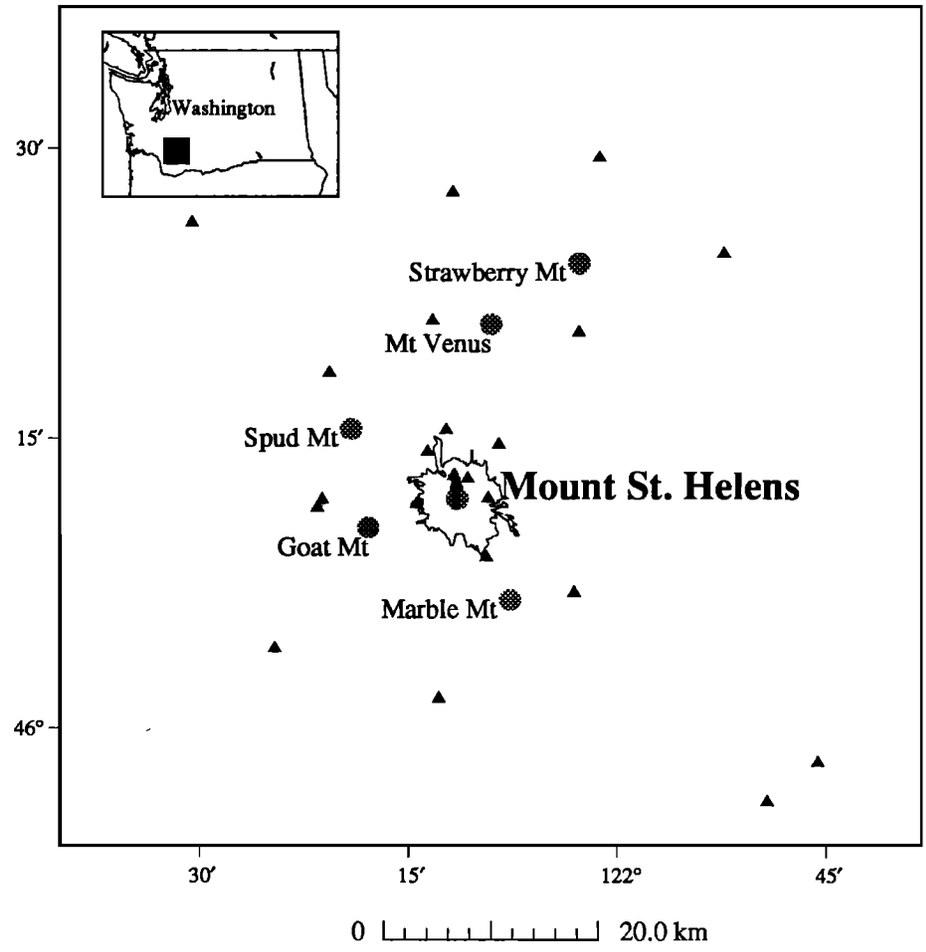

Fig. 1. Map view of target area showing station distribution. The inset shows the location of target area in Washington. Triangles are station locations, and labeled bullets identify major topographic highs in the area. The pre-1980 eruption tree line around Mount St. Helens is plotted for reference.

and ray paths from the sources to each observing station are calculated. The quantities modeled consist of observed travel times less travel times calculated through a one-dimensional reference model (i.e., a model with zero perturbations). These resulting time perturbations represent the line integrals of the slowness perturbation field along the ray paths. Denoting the length of the ith ray path in the jth block by a_{ij}, the travel time perturbation for that raypath b_i becomes $b_i = \sum a_{ij} x_j$, where x_j is the slowness perturbation in the jth block. The complete inverse problem can be expressed in the form of a large but sparse system of linear equations,

$$\mathbf{A}\,\mathbf{x} = \mathbf{b} \tag{1}$$

The classical least squares solution to (1) leads to the normal equations

$$\mathbf{A}^T\mathbf{A}\mathbf{x} = \mathbf{A}^T\mathbf{b}$$

a square, symmetric system that is guaranteed to have a solution that minimizes the squared misfit length, a functional denoted by

$$\| \mathbf{A}\mathbf{x} - \mathbf{b} \|^2$$

where $\|\cdot\|$ represents the Euclidean norm. However, the matrix $\mathbf{A}$ generally has small singular values, and $\mathbf{A}^T\mathbf{A}$ is typically highly ill-conditioned. One approach in dealing with this is to use the Levenberg-Marquandt method [*Crosson*, 1976*a*] and augment the system in (1) by a set of additional constraints in the following manner:

$$\begin{bmatrix} \mathbf{A} \\ \lambda\mathbf{I} \end{bmatrix} \mathbf{x} = \begin{bmatrix} \mathbf{b} \\ 0 \end{bmatrix} \tag{2}$$

where $\lambda\mathbf{I}$ is an $m \times m$ identity matrix multiplied by the constant λ, m being the number of model parameters (blocks) in the target. This leads to a damped least squares solution which minimizes the functional,

$$\|\mathbf{A}\mathbf{x} - \mathbf{b}\|^2 + \lambda^2\|\mathbf{x}\|^2$$

We would thus find the solution which minimizes the misfit of the data and has the smallest Euclidean length (weighted by λ).

If we assume that the slowness field that we are inverting for is a discrete version of a continuously varying slowness, we will want our solutions to have a certain measure of smoothness. The procedure of imposing constraints on ill-posed least squares inverse problems is often referred to as regularization. A discussion of regularization is given by *Hofmann* [1986], *Baumeister* [1987], and *O'Sullivan* [1986]. In our case, smoothness constraints can be imposed by minimizing a measure of the roughness of the model, where we have chosen the roughness to be

the second differential operator in the horizontal plane. In vector notation this is just the Laplacian operator, ∇^2. We augment the system in (1) by replacing **I** with **L** in (2),

$$\begin{bmatrix} \mathbf{A} \\ \lambda\mathbf{L} \end{bmatrix} \mathbf{x} = \begin{bmatrix} \mathbf{b} \\ 0 \end{bmatrix} \tag{3}$$

where **L** is the two-dimensional, finite difference Laplacian operator applied over horizontal planes in our model. Solving (3) by least squares is equivalent to a weighted minimization of the Laplacian operator at each point of the model in horizontal planes. In two dimensions this corresponds to the following equation for the jth block:

$$4*(j\text{th block slowness}) - \sum(\text{adjacent slowness}) =$$

$$4\,x_j - (x_{j+1} + x_{j-1} + x_{j+n} + x_{j-n}) = 0$$

where n is the number of blocks on the side of the model. Using this augmented system, we will minimize the following functional:

$$\|\mathbf{Ax} - \mathbf{b}\|^2 + \lambda^2(\mathbf{x}^T\mathbf{L}^T\mathbf{Lx}) = \|\mathbf{Ax} - \mathbf{b}\|^2 + \lambda^2\|\mathbf{Lx}\|^2$$

The parameter λ is used to adjust the relative weight of roughness verses misfit reduction as a tradeoff parameter. A discussion of the use of differential operators as roughening constraints is given by *Constable et al.* [1987], and the discrete Laplacian operator is introduced by *Young* [1971].

Because the data are not all equally accurate, it is desirable to weight down data that have higher uncertainties. Following the standard approach to weighted least squares [*Crosson*, 1976*a*; *Menke*, 1984], we multiply each row of $\mathbf{Ax} = \mathbf{b}$ by a weight proportional to the inverse of the estimated uncertainty in the datum. If the estimated uncertainty in the ith observed datum is σ_i, the weighting matrix **W** is defined by

$$\mathbf{W} = \left[\frac{1}{\sigma_1}, \frac{1}{\sigma_2}, \cdots, \frac{1}{\sigma_n}\right]\mathbf{I}$$

Finally, the system we are left to solve is (3) modified by **W**:

$$\begin{bmatrix} \mathbf{WA} \\ \lambda\mathbf{L} \end{bmatrix} \mathbf{x} = \begin{bmatrix} \mathbf{Wb} \\ 0 \end{bmatrix} \tag{4}$$

and the functional we minimize is

$$\|\mathbf{WAx} - \mathbf{Wb}\|^2 + \lambda^2\|\mathbf{Lx}\|^2$$

The uncertainties are estimated by a seismic analyst when the arrival time is picked. It should be noted that the errors in the data do not have a strictly normal distribution nor are they completely independent.

There are several methods available for finding solutions to large, sparse linear sets of equations that arise in problems of tomography. *Humphreys et al.* [1984], *Hearn and Clayton* [1986], and *Nakanishi* [1985] have all used various modifications of ART-backprojection techniques to successfully image parts of the upper crust in California and the South Pacific. *Spakman and Nolet* [1988] and *Scales* [1987] have recommended using a conjugate gradient method to solve the inverse problem. We have experimented with several methods and found that they produce quite similar results [*Lees and Crosson*, 1989]. In this study we present results using an algorithm originally proposed by *Paige and Saunders* [1982] called LSQR. It is based on a bidiagonalization of the system using Lanczos methods developed by *Golub and Kahan* [1965], followed by a QR decomposition to find the solution. The method is outlined by *Golub and Van Loan* [1983] and *Spakman and Nolet* [1988].

In principle, a nonlinear inversion could be obtained by using the laterally heterogeneous velocity model derived above to recalculate ray paths and then to relocate the hypocenters relative to the perturbed model. The process could then be iterated until the changes in the model, locations and ray paths become small. However, the amount of computation required to recalculate the three-dimensional ray paths is extremely large, and this step was not attempted. The question of whether such a nonlinear inversion converges is therefore beyond the scope of this study, and our results can be thought of as a first-order approximation.

The resolution of the inversion is primarily a function of the ray distribution. In the context of classical least squares, if **A** is the matrix that describes the way the rays sample the model blocks, the resolution matrix is $\mathbf{R} = (\mathbf{A}^T\mathbf{A})^{-1}\mathbf{A}^T\mathbf{A}$ [*Crosson*, 1976*a*]. For our modified version of least squares, $\mathbf{R} = (\mathbf{A}^T\mathbf{W}^T\mathbf{WA} + \lambda^2\mathbf{L}^T\mathbf{L})^{-1}\mathbf{A}^T\mathbf{W}^T\mathbf{WA}$. However, the sheer volume of data used in an inversion of this sort makes the calculation of the resolution matrix prohibitive. For this reason we resort to estimating the resolution by other means. One way to estimate the resolution is to examine the impulse response of the system for a typical block in critical regions [*Humphreys and Clayton*, 1988]. This is done by placing a unit perturbation in only the block of interest and performing forward modeling using the ray paths from the real data set. This synthetic data set is then inverted (using the same procedure as the real data inversion), and the result is the impulse response of the combined data set and inversion process for the given block. The impulse response relates how an anomaly present in a given block is spread into neighboring blocks. Ray coverage diagrams were used in conjunction with impulse responses of selected blocks to estimate the resolution at critical regions in the model.

For the same reasons outlined above, the model covariance matrix is also unavailable from a practical standpoint. In this case we applied a statistical technique called "jackknife" to estimate the standard errors of model parameters. Jackknife involves breaking the data set down into subsets, performing inversions on the subsets and calculating a standard error from the set of image vectors that result [*Mosteller and Tukey*, 1977; *Efron*, 1982]. The process is described as follows. First, an inversion is performed using all the data and the result is stored as a vector, $\hat{\mathbf{s}}_{all}$. Then the data is divided into k sets, each set leaving out a random $1/k$th portion of the data without replacement. A separate inversion is performed for each of the k subsets and the slowness image derived from each inversion is denoted $\hat{\mathbf{s}}_j$. From these "mini-inversions" a "pseudo-inversion," $\tilde{\mathbf{s}}_j$, is formed by the following linear combination:

$$\tilde{\mathbf{s}}_j = k\,\hat{\mathbf{s}}_{all} - (k-1)\,\hat{\mathbf{s}}_j$$

The pseudo-inversions thus represent information about the model that is explained by that portion of the data that was removed. Since each of the k subsets have a different nonoverlapping set of excluded data the variability of the model due to all the data is contained in the pseudo-inversions. The jackknife

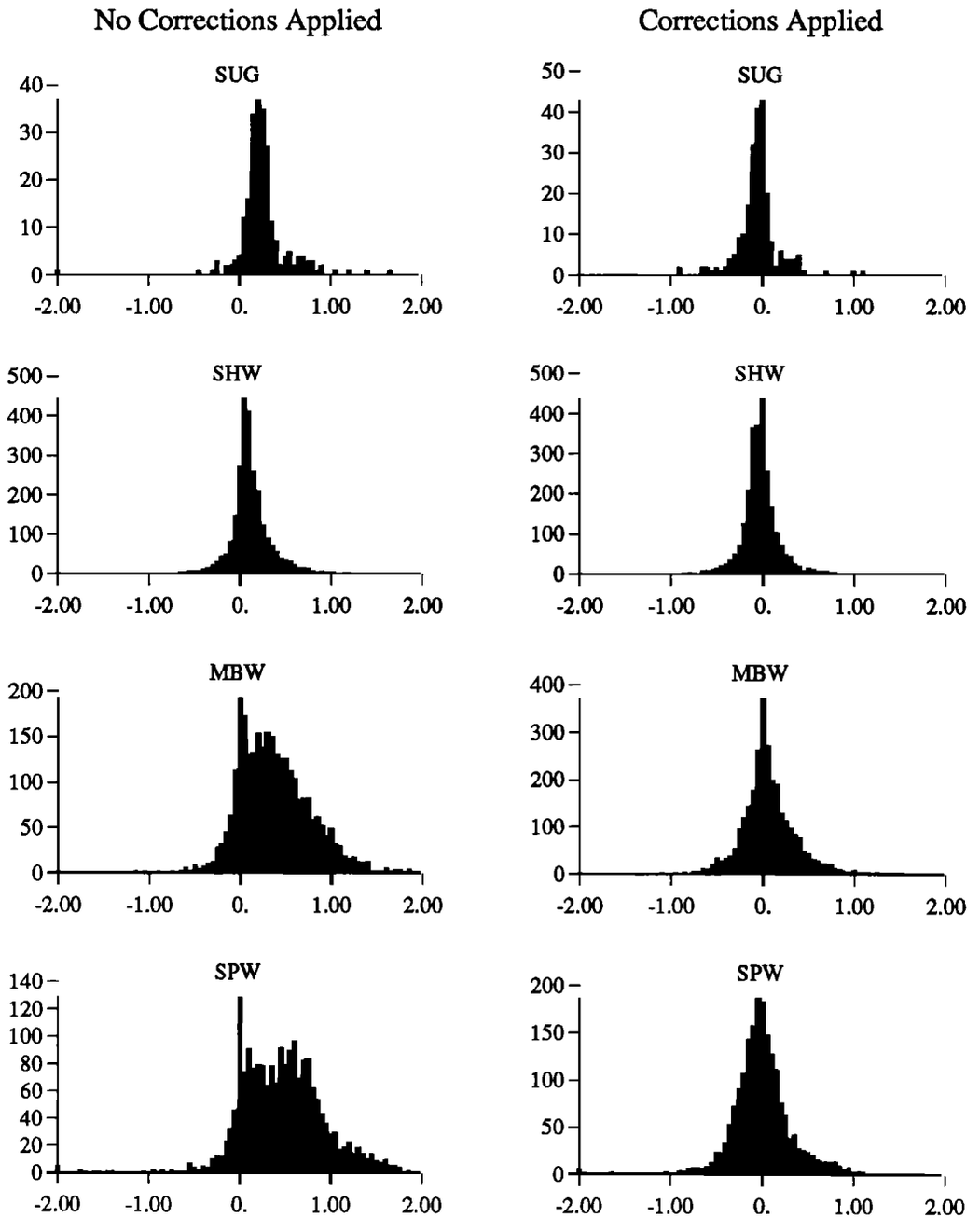

Fig 2. Histograms of station residuals. The horizontal axis is in seconds. On the left are the residuals for earthquakes located with no station corrections and on the right are the same residuals with corrections applied (the delay is indicated for each station). Notice the improvement after delays are incorporated.

estimate of the slowness is simply the average of the pseudo-inversions:

$$\bar{s} = \frac{\sum_{k} \bar{s}_j}{k}$$

which has variance,

$$v = \frac{\sum \bar{s}_j^2 - \frac{1}{k}(\sum \bar{s}_j)^2}{k\,(k-1)}$$

From this the standard error is $E_\sigma = \sqrt{v}$. This will be an estimate of the variability of the model and can be used to project how large the errors are in each block of the target. This approach is similar to the bootstrap technique suggested by *Willmott et al.* [1985] only in the bootstrap case one samples from the data with replacement, and variability is estimated from mini-inversions as opposed to pseudo-inversions.

For the classical jackknife, k would be the number of rays in the data set, meaning, leaving out one ray for each pseudo-inversion [*Mosteller and Tukey*, 1977]. However, this would involve performing thousands of inversions, a very time consum-

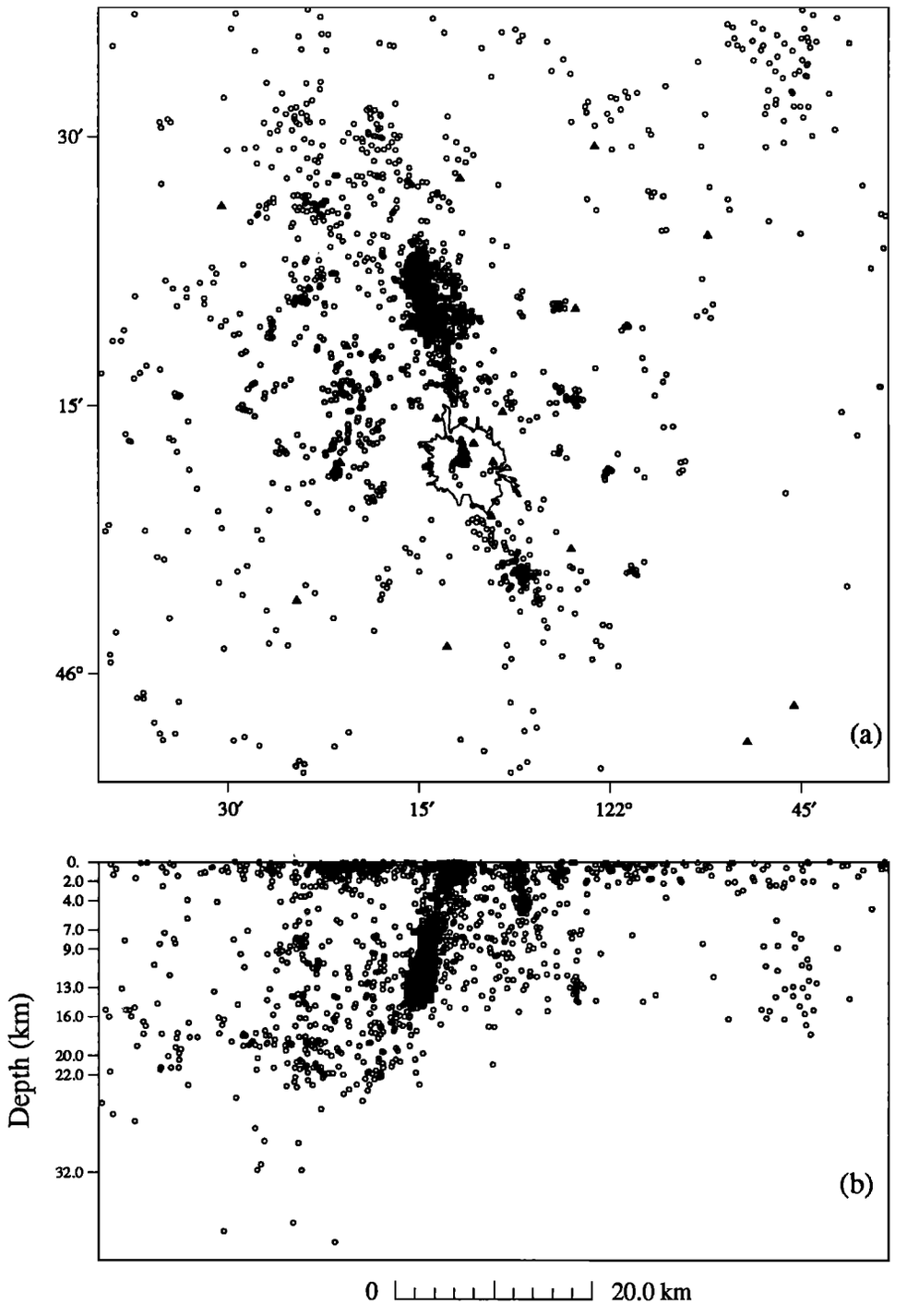

Fig. 3. (*a*) Epicenter map and (*b*) east-west vertical projection of earthquake sources within target area. The SHZ is clearly evident by the high seismicity lineation extending north of Mount St. Helens.

ing operation. A compromise can be struck if we assume that the variability in the pseudo-inversions will be represented in far fewer partitions of the data. Unfortunately, there is no known general method for choosing the number of partitions, k, that should be used to adequately encompass the variability of the data. In this study, for example, only 30 partitions were used. This represented 3.3% of the total or roughly 580 rays excluded per mini-inversion.

An alternative to this approach [*Humphreys and Clayton*, 1988] is to assume a distribution of noise for the data and to create artificial data with these noise characteristics. These data are inverted, and the outcome is inspected as a representation of the model uncertainty. The advantage of the jackknife approach is that it is nonparametric; that is, we are using the data themselves to estimate the covariance and have made no assumptions about how the data are distributed.

DATA SELECTION

The data used in this study were gathered for the time period 1972-1987 from the western Washington seismic network operated by the University of Washington. Short-period seismic stations are located within the target region surrounding Mount St. Helens shown in Figure 1. Station density has been sufficient since the 1980 eruption for detailed inversion studies. The following criteria were used for choosing events from the data base: (1) locations within the target volume (excluding events located in a small region centered on the Mount St. Helens crater to prevent heavy biasing from highly localized, shallow data associated with eruptions and aftershocks of 1980); (2) azimuthal gap < 180°; (3) minimum source-receiver distance < 50 km; (4) rms residual < 0.5 s; and (5) number of picks > 5 for each event. Station corrections must be determined to remove the effect of structure in the immediate vicinity of the stations. Since our models are adjusted to a constant elevation datum, the station correction will include the effects of variation in elevation between stations. To determine station corrections, we plotted histograms of travel time residuals from all the data in the data base (including data outside of our target volume). Because the distribution of residuals at each station was often skewed or bimodal, the histograms were inspected visually, and a time delay was chosen by inspection to remove the average of the largest clusters of residuals. Station corrections were then incorporated in the location procedure and residuals recalculated and plotted. This process was iterated until a stable set of residuals was determined (approximately five iterations). Four examples of residual histograms are presented in Figure 2. On the left are residual distributions calculated with locations using no station correction and the right hand side shows the same residuals after the final station correction has been applied. Notice the the shift and narrowing of the distributions after station corrections have been accounted for. The event locations using the final station corrections were considered fixed (or known) for the subsequent velocity inversions.

Figure 3*a* shows the areal distribution of the sources, and Figure 3*b* is a projection of the hypocenters onto the east-west vertical cross section. We excluded all rays that did not lie entirely within the target model. Approximately 98% of the residuals were less than 1 s; however, some rays had unrealistically large residuals (>2 s) which were considered outliers and excluded from the data set. Some stations had so few rays (<30) that they were also excluded. The remaining data set included 17,659 rays recorded at 21 stations from 2023 hypocenters. The heaviest coverage was in the range of 2-10 km depths, and the deepest event used was at 40 km depth. The earthquake coverage was not homogeneous due to the preponderance of events located in the SHZ. This was partially compensated for by weighting as described in the previous section.

TABLE 1. Velocity Model

Depth	P-velocity	P-slowness
0.0	5.4	0.185
4.0	6.38	0.157
9.0	6.59	0.152
16.0	6.73	0.149
20.0	6.86	0.146
25.0	6.95	0.144
32.0	6.90	0.145
41.0	7.80	0.128

Based on least squares model developed by *Crosson* [1976*b*]. The velocities and boundaries used in the inversion routine were interpolated from this model.

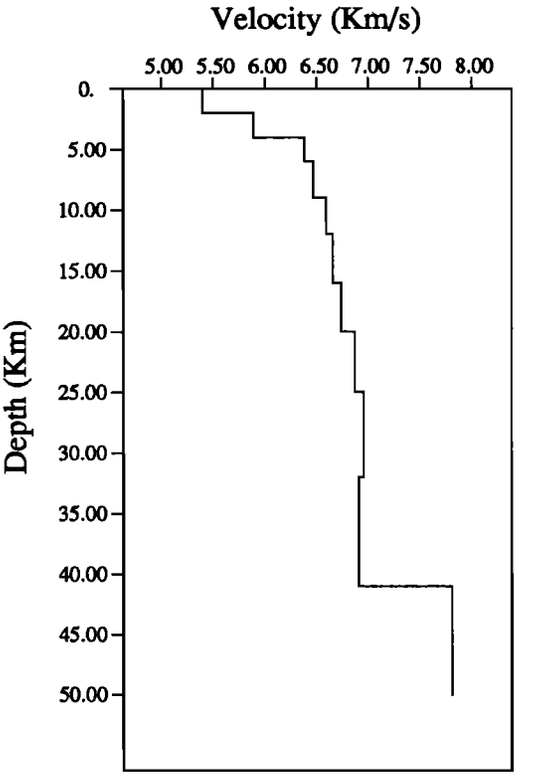

Fig. 4. One-dimensional layered reference model used in inversion. The model is interpolated from the one-dimensional model derived by least squares.

The initial reference model (Table 1) was derived from a least squares model [*Crosson*, 1976*b*] that was interpolated to a finer depth spacing to increase the parameterization in the shallow layers. This also made the blocks nearly cubical for the top layers. The velocities for these layers were interpolated from the least squares model by taking weighted averages. The one-dimensional interpolated model (Figure 4) was used to relocate all the earthquakes in the selected data set as well as a starting model for the inversion. We found by experiment with other models that the end result was not highly sensitive to the assumed reference model provided new station corrections and hypocenter locations were computed.

RESULTS OF INVERSION

In Figure 5 we show the results of the tomographic inversion. Each figure represents the slowness perturbation in a horizontal layer of the model. Note that the layers are of slightly different thickness, although each block is 2 km × 2 km horizontally. The gray shading represents levels of percent perturbation from the reference slowness of the layer. Since velocity is the reciprocal of slowness, dark areas (high slowness) represent low velo-

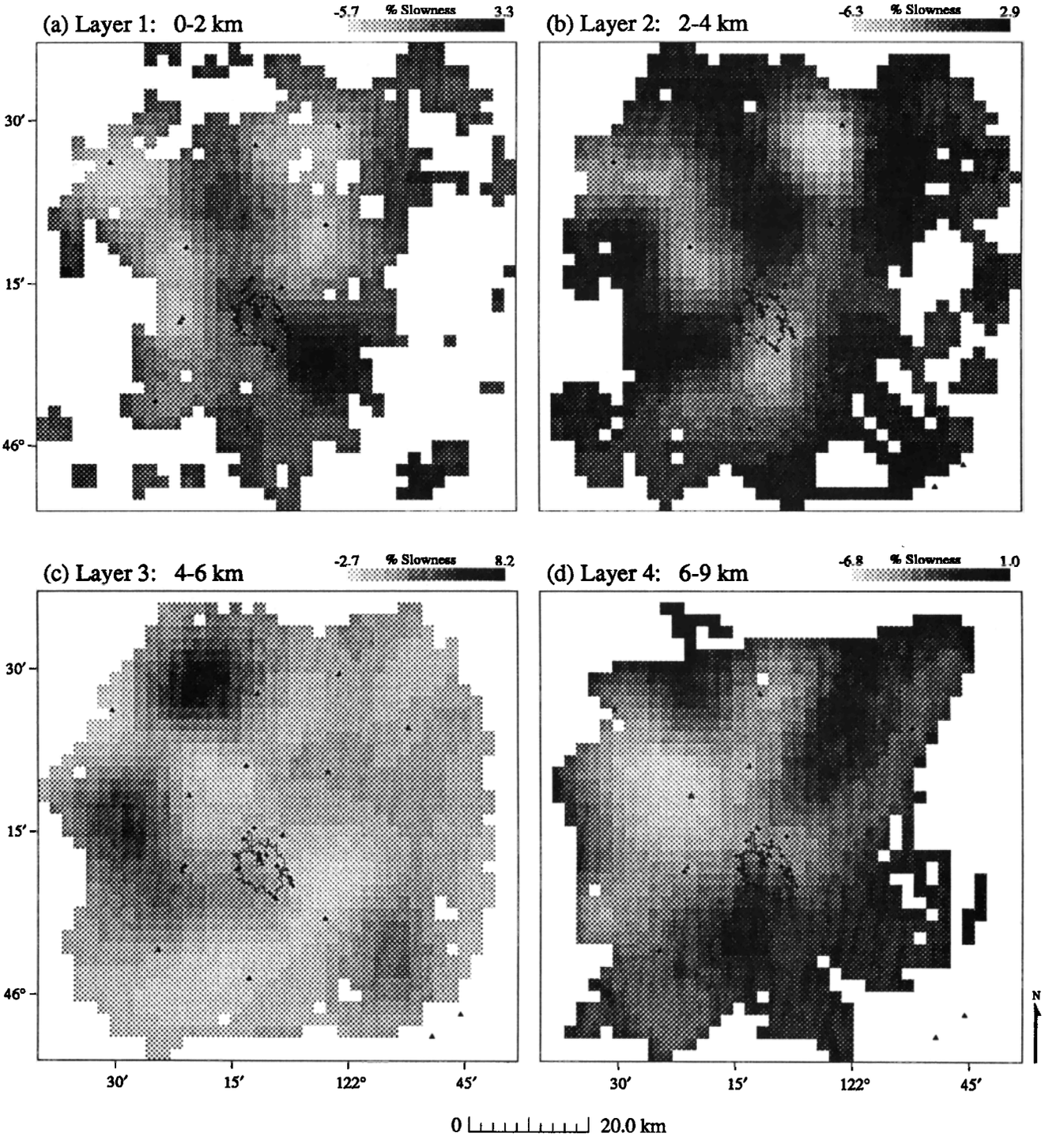

Fig. 5. Three-dimensional tomographic inversion for lateral variations in slowness perturbation. Each figure represents a horizontal slab in the earth. Gray shades represent percent perturbations from the reference model (Figure 4), such that light colored regions reflect high velocity and dark regions are low velocity. Dark triangles are station locations as illustrated in Figure 1.

city and light areas are relatively high velocity. Regions or blocks which are unshaded have not been sampled by any rays, indicating the extent of ray coverage. The outline of the pre-eruption tree line around Mount St. Helens as well as the stations have been plotted for geographical reference.

Anomalies present in the top layer (Figure 5*a*) have the appearence of shorter wavelength than we believe are resolvable. This is due to the fact that all the rays must terminate at one of the stations at the surface and very local anomalies are generated in the immediate vicinity of the stations where rays are clustered

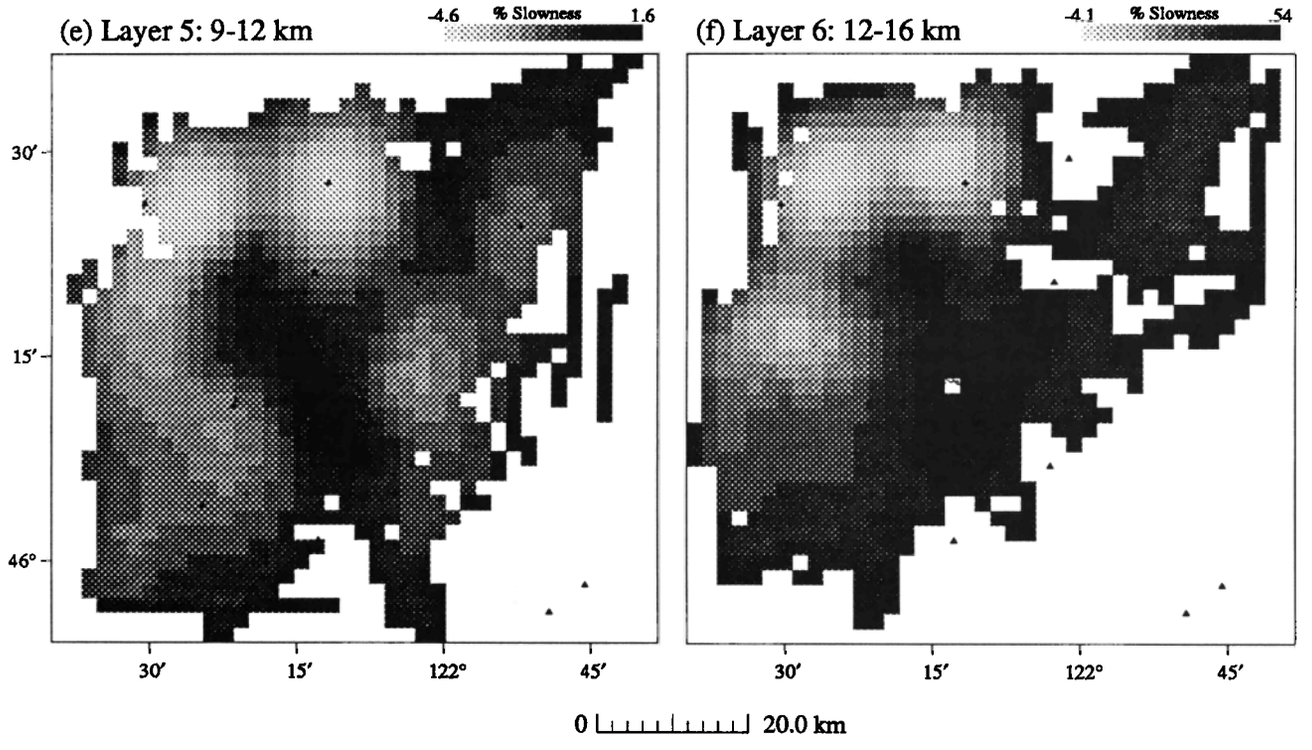

Fig. 5. (continued)

together. Anomalies in the top layer therefore represent local structure beneath the station that has not been accounted for in the station correction described in the previous section. For this reason the discussion below emphasizes the structure below the surface layer.

An impulse response kernel for a block located in layer three directly north of St. Helens is displayed in Figure 6. A spike of value 1 was put into the block that is outlined in white (Figure 6*b*) and artificial data were generated using the rays of the real data. The output was then inverted in the same fashion as the actual data. The result indicates that the lateral resolution in layer three (Figure 6*b*) is excellent (three blocks) near the center of the model. Because there are relatively few layers, resolution in the vertical dimension is more difficult to achieve. The anomaly is spread into the layers above and below in a NNE direction. This is due to the high seismicity located in the SHZ where blurring has occurred. Note, however, that the amplitude of the anomaly in the layers above and below the spike are attenuated by about a third of the height of the center block. This resolution is typical of the central portion of the model in layers 2-5. On the edges the resolution is degraded.

In general, the errors in this model (Figure 7) are not large enough to change the sign of the gross anomalies apparent in the inversion. For example, the anomaly at the Spirit Lake pluton (46°30'N-122°W) is about -6.3%. But the predicted standard error here is very small, less than 0.8%. If the errors are assumed to be uncorrelated, this would indicate that at least the sign of the velocity structure is well constrained by the three dimensionl inversion. Since the errors are correlated in our case (through, for example, earthquake mislocations), we expect the model errors to be slightly higher.

DISCUSSION AND CONCLUSIONS

The prominent anomalies apparent in the three dimensional model show a remarkable correlation with the surface geology and other geophysical measurements. *Evarts et al.* [1987] has mapped out surface expressions of such features as the Spirit Lake pluton trending NNE from the crater of St. Helens and the Spud Mountain pluton which trends NNW. A lineation of plug domes and extinct vents runs in an east-southeast direction from the crater and takes a slight bend to the northwest north of St. Helens. These features are apparent on the aeromagnetic map of *Finn and Williams* [1987] (reproduced here as Figure 8) where high magnetic anomalies are recorded at Spirit Lake and Spud Mountain, and a low trough is evident in between, at the location of the St. Helens seismic zone (SHZ) [*Weaver and Smith*, 1983]. The seismic anomalies in the first three layers (0-6 km, Figures 5*a*-5*c*) of the three dimensional model presented here reflect the same structures. A high-velocity zone maps directly into the two plutons located north of St. Helens with a prominent low-velocity zone at the SHZ separating them. The Goat Mountain complex is evident as a low-velocity region. An enlarged version of Figure 5*b* is provided in Figure 9, showing these features superimposed on the slowness anomalies for clarity. At the crater of St. Helens a high-velocity anomaly of 2.1% contrasts with a low-velocity anomaly of 2.5% directly to the north. A similar pattern has been observed by *Fehler* [1985] in a joint inversion of earthquake locations and station delays using 32 shallow events near the crater. The anomaly appears to have reversed by a depth of 6-9 km (Figure 5*d*) where a 0.6% low-velocity is evident. In the deeper layers (9-16 km depth) there is a strong low velocity anomaly beneath the crater which may be indicative of modern magma accumulations.

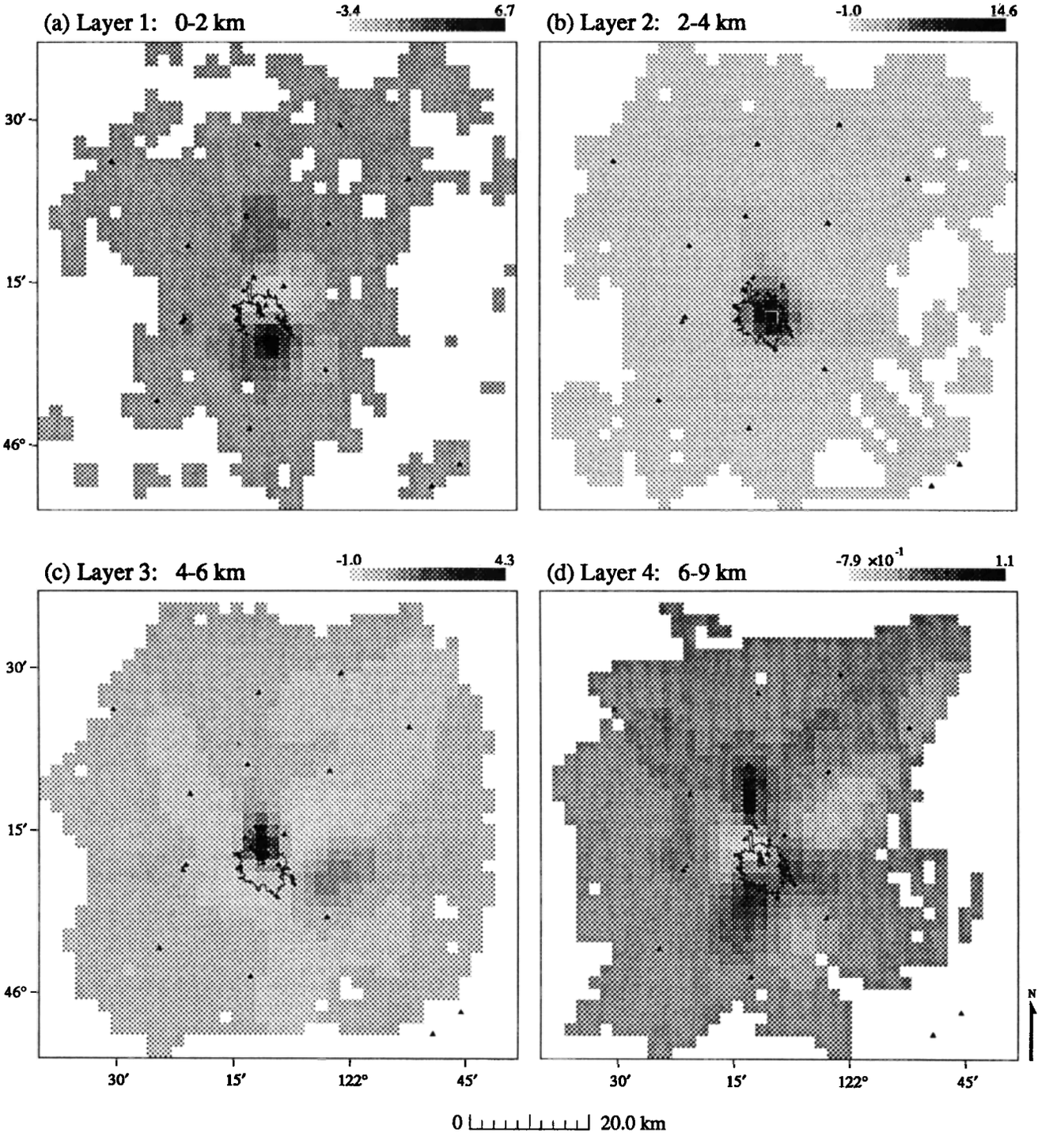

Fig. 6. Resolution impulse response for highlighted block located in near the center of layer 2. Perfect resolution would produce 100% in this block, but after forward and inverse modeling only 15% of the amplitude remains with the rest spread throughout the model.

The low-velocity anomaly that runs along the SHZ is apparent at virtually all depths. In the deeper layers it is the major outstanding feature in the model. This slower zone coincides with high seismicity and is presumed to be the lineation of a crustal zone of weakness characterized by strike-slip faulting extending north-northwest from Mount St. Helens [*Weaver et al.*, 1987]. *Weaver et al.* [1987] suggest that Mount St. Helens is situated at the corner of a bend in the SHZ where it trends to the southeast toward Marble Mountain. The velocity anomalies in our model below the first layer do not reflect such a trend.

There is strong evidence that the boundaries delineated by the seismic velocity inversions represent important subsurface inter-

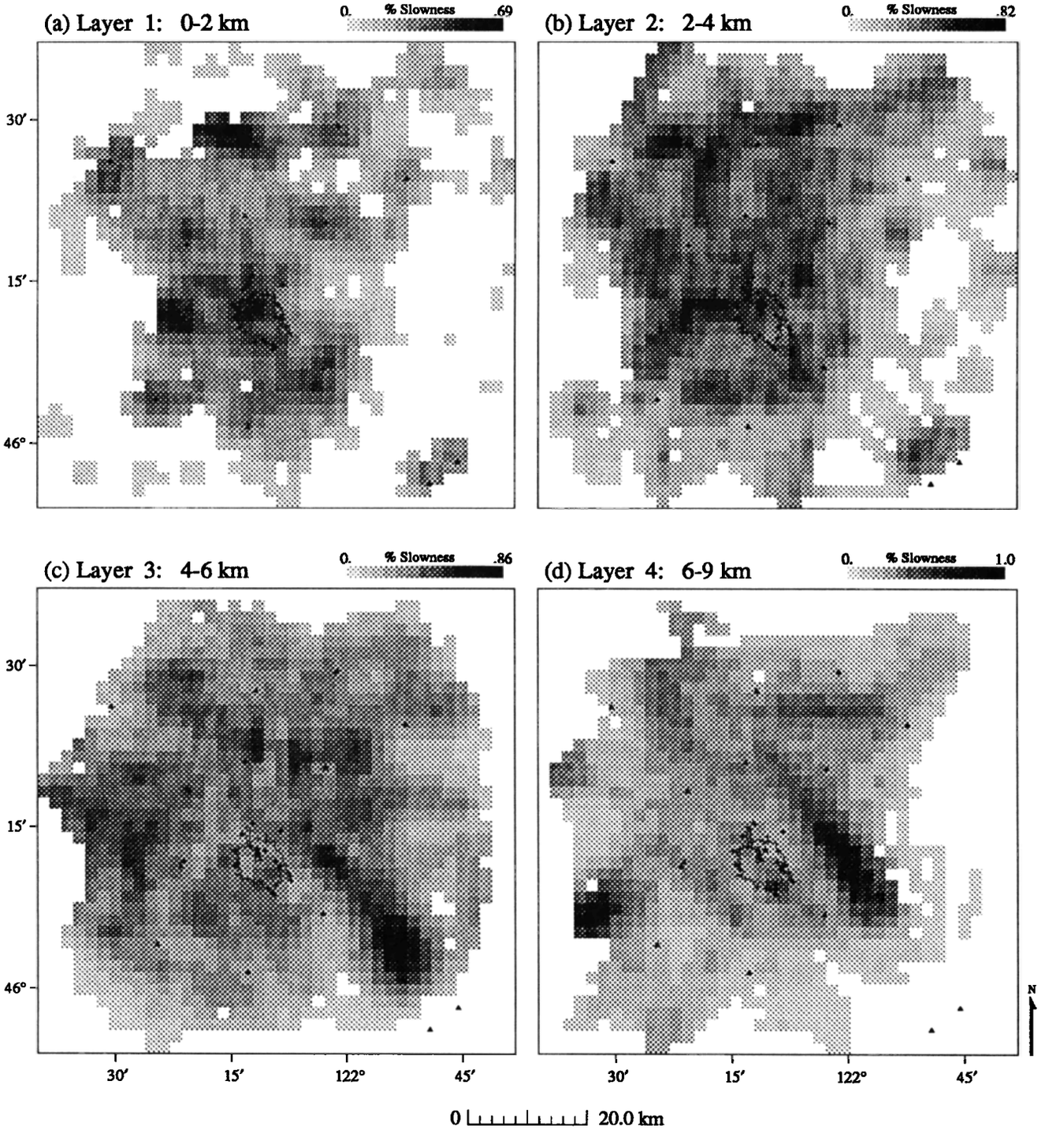

Fig. 7. Estimated standard error using the jackknife for layers 1-4. Shades of gray represent error in percent slowness perturbation where dark areas have higher standard error.

faces separating rocks of significantly varying properties. These structures are evident in the surface exposure and in other geophysical studies, such as the aeromagnetic and gravity surveys. If we assume that zones of low velocity reflect the presence of fracturing, magmatic intrusion, fluids, or high heat source, then the SHZ north of Mount St. Helens may be the major tectonic feature of this region. We speculate that this zone is a weak boundary, separating distinct geologic terrains, that is reactivated under regional tectonic stress. This would explain the affinity of both earthquakes and volcanic conduits (e.g., Mount St. Helens) for this zone. The vents and plug domes of the Goat Mountain complex also appear to exhibit low velocities; however, the Marble Mountain region exhibits low-velocity structure only in the shallowest zones (0-2 km). At depth (6-12 km) the low-velocity

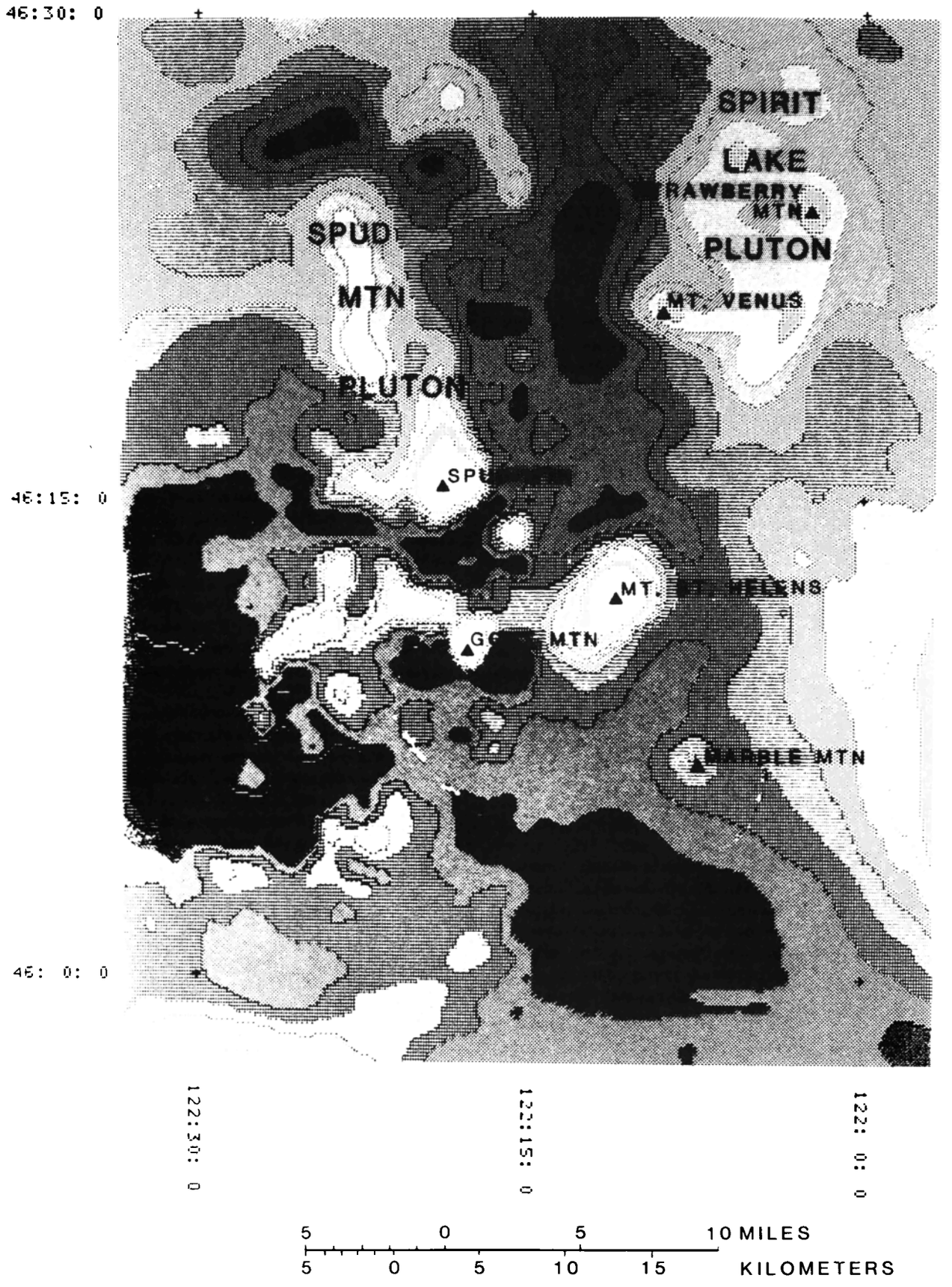

Fig. 8. Regional aeromagnetic map reduced to pole from *Finn and Williams* [1987]. Units range from -1500 nT (dark) to 1600 nT (light). The anomalies here correlate with the velocity anomalies at 2-4 km depth (Figure 5b).

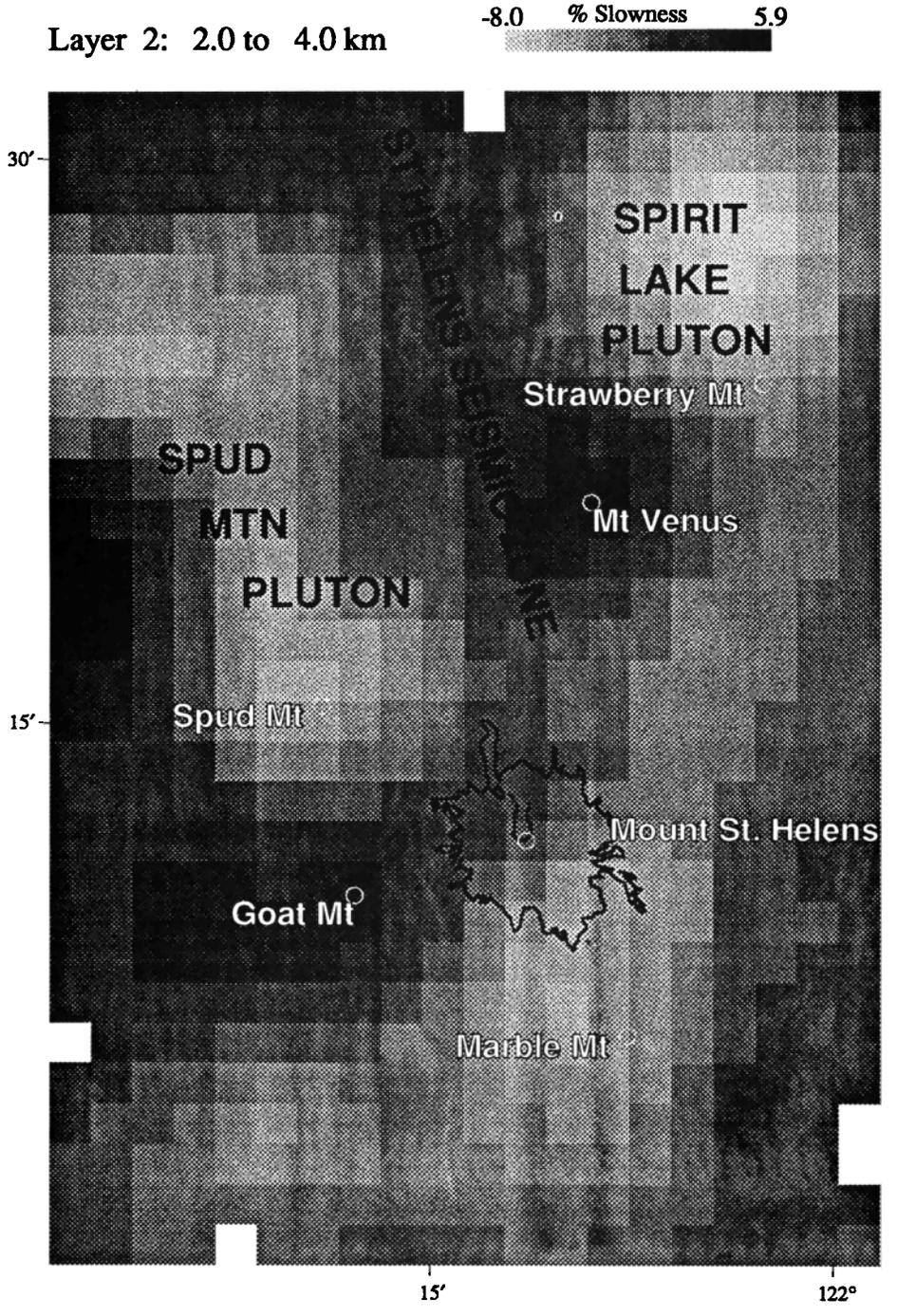

Fig. 9. A close up of Figure *5b* to match the scale of the aeromagnetic anomalies in Figure 8. Important features discussed in the text are labeled for clarity.

anomaly appears immediately south of the crater and shows little evidence of bending to the southeast. The high-velocity plutons at Spirit Lake and Spud Mountain represent consolidated, brittle material that is significantly more impervious to fluid injection. These plutons are separated by the strike-slip faulting of the SHZ. Because the presence of the quartz-dioritic plutons appears to be consistent in the deeper layers they may constrain the zone of weakness in the crust that produces the SHZ. In other localities, this technique of using local earthquakes for tomographic imaging may prove to be useful in locating areas of crustal weakness and thus potential seismic hazards. Such information should also prove of great value in studying the processes and structure of volcanic systems.

Acknowledgements. The authors are grateful to Antonio Possolo and Torquil Smith for many helpful discussions. Steve Malone, Ken Creager, Michael Fehler, and one anonymous reviewer contributed helpful suggestions to improve the manuscript. This work was supported by USGS grants 14-08-0001-G1080 and 14-08-0001-G1390 and USGS contract 14-08-0001-22169.

REFERENCES

Aki, K., A. Christoffersson, and E.S. Husebye, Determination of the three-dimensional seismic structure of the lithosphere *J. Geophys. Res.*, *82*, 277-296, 1977.

Baumeister, J., *Stable Solution of Inverse Problems*, Friedr. Vieweg, Braunschweig, Federal Republic of Germany, 1987.

Constable, A.C., R.L. Parker, and C.G. Constable, Occam's inversion: A practical algorithm for generating smooth models from electromagnetic sounding data, *Geophysics, 52* (3), 289-300, 1987.

Crosson, R.S., Crustal structure modeling of earthquake data, 1, Simultaneous least squares estimation of hypocenter and velocity parameters, *J. Geophys. Res., 81*(17), 3036-3046, 1976a.

Crosson, R.S., Crustal structure modeling of earthquake data, 2, Velocity structure of the Puget Sound region, Washington *J. Geophys. Res., 81*, 3047-3054, 1976b.

Dickinson, W.R., Sedimentary basins developed during evolution of Mesozoic-Cenozoic arc-trench system in western North America, *Can. J. Earth Sci., 13*, 1268-1283, 1976.

Efron, B., The Jackknife, the Bootstrap and Other Resampling Plans, *Society for Ind. and Applied Mathematics*, Philadelphia, Pa., 1982.

Evarts, R.C., R.P. Ashley, and J.G. Smith, Geology of the Mount St. Helens area: Record of discontinuous volcanic and plutonic activity in the Cascade arc of southern Washington, *J. Geophys. Res., 92*, 10,155-10,169, 1987.

Fehler, M., Locations and spectral properties of earthquakes accompanying an eruption of Mount St. Helens, *J. Geophys. Res., 90*, 12,729-12,740, 1985.

Finn, C., and D.L. Williams, An aeromagnetic study of Mount St. Helens, *J. Geophys. Res., 92*, 10,194-10,206, 1987.

Golub, G.H., and W. Kahan, Calculating the singular values and pseudoinverse of a matrix, *SIAM J. Numer. Anal., 2*, 205-224, 1965.

Golub, G.H., and C.F. Van Loan, *Matrix Computations*,, The John Hopkins University Press, Baltimore, Md., 1983.

Hammond, P.E., Reconnaissance geologic map and cross sections of southern Washington Cascade Range, latitude 45°30'-47°15'N longitude 120°45'-122°22.5'W, scale 1:125,000, Dep. of Earth Sci., Portland State Univ., Oreg, 1980.

Hearn, T.M., and R.W. Clayton, Lateral velocity variations in southern California, 1, Results for the upper crust from *Pg* waves, *Bull. Seismol. Soc. Am., 76*, 495-509, 1986.

Hofmann, B., *Regularization for Applied Inverse and Ill-Posed Problems*, Teubner-Texte, Leipzig, German Democratic Republic, 1986.

Humphreys, E., and R.W. Clayton, Adaptation of back projection tomography to seismic travel time problems, *J. Geophys. Res., 93*, 1073-1085, 1988.

Humphreys, E.D., R.W. Clayton, and B.H. Hager, A tomographic image of mantle structure beneath southern California, *Geophys. Res. Lett., 11*, 625-627, 1984.

Lees, J.M., and R.S. Crosson, Bayesian ART versus conjugate gradient methods in tomographic seismic imaging: An application at Mount St. Helens, Washington, in *Spatial Statistics and Imaging: Proceedings of the 1988 AMS-IMS-SIAM Summer Research Conference*, in press 1989.

McBirney, A.R., Volcanic evolution of the Cascade Range, *Annu. Rev. Earth Planet. Sci., 6*, 437-456, 1978.

Menke, W., *Geophysical Data Analysis: Discrete Inverse Theory*, Academic, San Diego, Calif., 1984.

Mosteller, F., and J.W. Tukey, *Data Analysis and Regression*, Addison-Wesley, Mass., 1977.

Mullineaux, D.R., and D.R. Crandell, The eruptive history of Mount St. Helens, *U.S. Geol. Surv. Prof. Pap., 1250*, 3-16, 1981.

Nakanishi, I., Three-dimensional structure beneath the Hokkaido-Tohoku region as derived from a tomographic inversion of *P*-arrival times, *J. Phys. Earth, 33*, 241-256, 1985.

O'Sullivan, F., A statistical perspective on ill-posed inverse problems, *Stat. Sci., 1*(4), 502-527, 1986.

Paige, C.C., and M.A. Saunders, LSQR: An algorithm for sparse linear equations and sparse least squares, *Trans. Math. Software, 8*, 43-71, 1982.

Phillips, W.M., Geologic map of the Mt. St. Helens quadrangle, Washington and Oregon, scale 1:100,000, *Wash. Div. Geol. Earth Resour. Open File Rep. 87-4*, 1987.

Scales, J.A., Tomographic inversion via the conjugate gradient method, *Geophysics, 52*, 179-185, 1987.

Spakman, W., and G. Nolet, Imaging algorithms, accuracy and resolution in delay time tomography, in *Mathematical Geophysics*, pp. 155-187, D. Reidel, Hingham, Mass., 1988.

Stanley, W.D., C. Finn, and J.L. Plesha, Tectonics and conductivity structures in the southern Washington Cascades, *J. Geophys. Res., 92*, 10,179-10,193, 1987.

Swanson, D.A., and G.A. Clayton, Generalized geologic map of the Goat Rocks wilderness and roadless areas (6036, parts A, C, and D), Lewis and Yakima counties, Washington, scale 1:48,000, *U.S. Geol. Surv. Open File Map, 83-357*, 1983.

Weaver, C.S., and S.W. Smith, Regional tectonic and earthquake hazard implications of a crustal fault zone in southwestern Washington, *J. Geophys. Res., 88*, 10,371-10,383, 1983.

Weaver, C.S., W.C. Grant, and J.E. Shemeta, Local crustal extension at Mount St. Helens, Washington, *J. Geophys. Res., 92*, 10,170-10,178, 1987.

Williams, D.L. , G. Abrams, C. Finn, D. Dzurisin, D.J. Johnson, and R. Denlinger, Evidence from gravity data for an intrusive complex beneath Mount St. Helens, *J. Geophys. Res., 92*, 10,207-10,222, 1987.

Willmott, C.J., S.G. Ackleson, R.E. Davis, J.J. Feddema, K.M. Klink, D.R. Legates, J. O'Donnell, and C.M. Rowe, Statistics for the evaluation and comparison of models, *J. Geophys. Res., 90*, 8995-9005, 1985.

Young, D.M., *Iterative Solution of Large Linear Systems*, Academic, San Diego, Calif., 1971.

R. S. Crosson and J. M. Lees, Geophysics Program, AK-50, University of Washington, Seattle, WA 98195.

(Received June 29, 1988;
revised December 27, 1988;
accepted December 27, 1988.)